Contact damage in porcelain/Pd-alloy bilayers

Hong Zhao, Xiaozhi Hu, and Mark B. Bush
Department of Mechanical and Materials Engineering, The University of Western Australia, Nedlands, WA 6907, Australia

Brian R. Lawn
Materials Science and Engineering Laboratory, National Institute of Standards and Technology, Gaithersburg, Maryland 20899

(Received 23 July 1999; accepted 6 December 1999)

An analysis is made of contact damage in brittle coatings on metal substrates, using a case study of a dental porcelain coating of thickness between 0.1 and 1 mm fused onto a Pd alloy base, with spherical indenter of radii 2.38 and 3.98 mm. At large coating thicknesses (>300 μm), the first damage takes the form of surface-initiated transverse cone cracks outside the contact. At small coating thicknesses (<300 μm), the first damage occurs as yield in the substrate, with attendant formation of subsurface transverse median cracks in the coating. At high loads and thin coatings, both forms of transverse cracking occur, along with subsequent delamination of the ceramic/metal interface, signalling impending failure. Conditions for avoiding such transverse cracking are considered in terms of minimum coating thicknesses and maximum sustainable contact loads. General implications concerning the design of brittle coating systems for optimum damage resistance are considered, with special reference to dental crowns.

I. INTRODUCTION

Layer structures composed of dissimilar materials are frequently encountered in engineering applications, as well as in nature.[1] Ceramic-on-metal layer structures, in particular, are developed for high damage tolerance applications in coatings on cutting tools,[2] thermal barrier coatings,[3,4] engine components,[5] etc. Ceramic/metal layer structures are also commonly used as crowns and bridges in restorative dentistry,[6] making use of the ceramic coating for wear resistance and aesthetics, the metal for rigidity, and the composite ceramic/metal bilayer for protection of a soft (but tough) inner dentin core.[7] Despite this broad range of applications, our fundamental understanding of failure modes in ceramic/metal layer structures, particularly in cases where the interlayer bonding is sufficient to avert delamination,[8] remains limited.

Structures containing brittle coating components are especially susceptible to damage in high-stress, concentrated loading applications.[9–11] Considerable recent attention has been given to this kind of loading, specifically using spherical (Hertzian) contacts, in the context of design of bilayer structures with brittle coatings.[2,7,8,12–24] In such contact configurations, energy from the loading system is partitioned between fracture in the brittle overlayer and quasi-plasticity in the underlayer. A key feature of the design in ceramic/metal layer structures is a strongly bonded interface, to avoid any delamination. Coating failure then results from the initiation and propagation of transverse cracks, either from the top surface (cone cracks) or lower surface (median cracks).[8] The median crack system becomes increasingly dominant as the coating thickness and the substrate hardness diminish.[25]

In this paper we use sphere contacts to investigate the modes of coating fracture in a brittle ceramic on a metal base, with the aim of determining design conditions for optimum fracture resistance. We choose as a case study a porcelain on a palladium alloy, for ease in preparation and relevance to restorative density. Questions as to maximum sustainable loads and minimum coating thicknesses for avoidance of transverse cracking are addressed. Optimization of relative material properties, particularly in the context of elastic and plastic mismatch, is also considered.

II. LAYER PREPARATION AND TESTING PROCEDURE

Porcelain/palladium-alloy bilayers were prepared for indentation testing in the configuration of Fig. 1, following standard routines practiced by dental technicians in the construction of porcelain-fused-to-metal crowns. This particular ceramic/metal combination has low thermal mismatch, avoiding the generation of significant re-

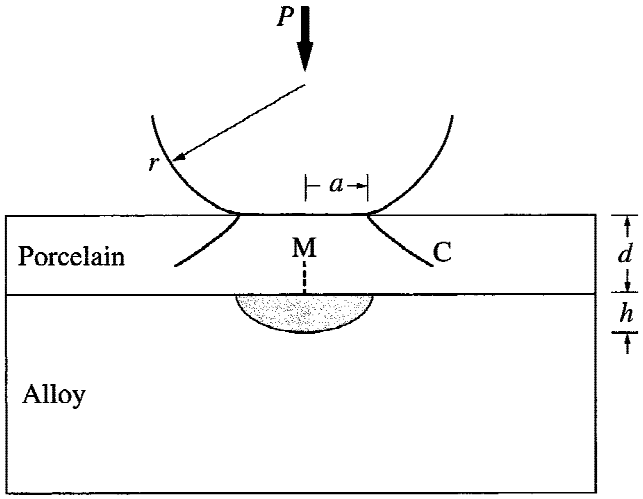

FIG. 1. Schematic of contact with sphere of radius r at load P on ceramic/metal bilayer, coating thickness d, with resultant contact radius a. Above critical loads, contact produces transverse cone (C) and median (M) cracks in coating, and yield zone, depth h, in substrate.

sidual stresses in the coating.[26,27] Palladium (Pd) alloy pellets (Argipal, 81.5% PD, 14.5% Tin, 3.5% GA, 0.5% Ru, Argen, San Diego, CA) were melted at 1300–1400 °C and cast into substrate blocks 20 × 15 × 3 mm. These blocks were then ground flat on opposite faces, oxidized at 960 °C, and finally sandblasted to provide good bonding for the ensuing coating. Porcelain powder (VITA VMK68N, Vita Zahnfabrik, Bad Säckingen, Germany) was mixed in a slurry and applied to the substrates with a paintbrush, in sequential layers of no more than 300 μm each. Each layer was sintered according to the following firing cycle, according to manufacturer's specifications: (i) heat to 600 °C in air and hold for 6 min, (ii) heat to 960 °C under vacuum and hold for 2 min, (iii) cool slowly in air. The top surfaces of the porcelain coatings were ground and polished with 1 μm diamond paste to specified thicknesses.

Bonded-interface specimens were employed to reveal subsurface damage patterns in the bilayers.[28,29] Specimens were cut in two halves parallel to their long dimensions, polished at the cut surfaces, and bonded back together with adhesive (Loctite Corp., Newington, CT). The top surface was then repolished to provide a flat surface for indentation. After indentation, the bonded specimens were immersed in acetone to dissolve the adhesive, separated into their two halves, and viewed in an optical microscope. Coating thicknesses were measured from the sections in the optical microscope. The validity of the bonded-interface technique in its capacity to provide a faithful representation of contact damage has been documented.[21,30]

Indentation tests were carried out on the top porcelain surfaces of the coated specimens using tungsten carbide (WC) spheres of radius $r = 2.38$ and 3.98 mm. The indenters were mounted in the crosshead of an Instron testing machine (Instron 1122, Canton, MA), and driven at a crosshead speed 0.2 mm min^{-1} to peak loads up to $P = 1400$ N. All indentation tests were carried out in air. Some tests were performed on the as-prepared bilayer surfaces, others on bonded-interface specimens by indenting along the trace of the interface at the top surface before separating into the constituent halves. The surfaces containing the indentations were gold coated and viewed in the optical microscope using Nomarski contrast.

Critical loads for the onset of damage were measured by post-contact observation of the indented specimens. In these tests, series of indentations at ever-increasing loads were made in lines along the specimen surfaces. The critical value P_C for cone crack initiation at the top surface of the porcelain coating was measured as the load range over which the cone first appeared as a small arc immediately outside the contact and then completed itself in a full trace around the contact circle. The critical value P_Y for yield in the metal substrate was determined by measuring the depth h (Fig. 1) at any given load P directly from bonded-interface section views of the plastic zones, and extrapolating the data back to zero depth.

Indentation stress–strain curves were determined from measurements of contact radii a at specified loads P on the bilayer top surfaces, yielding indentation stress, $p_0 = P/\pi a^2$, as a function of indentation strain, a/r. In these tests, the specimen surfaces were gold-coated prior to indentation, enabling measurement of the contact radii from residual impressions in the gold, using Nomarski contrast.[31]

III. RESULTS

A. Contact damage modes in bilayers

Figure 2 shows contact damage patterns in bonded-interface porcelain/Pd-alloy bilayer specimens, from indentations by a WC sphere of radius $r = 2.38$ mm at load $P = 1000$ N. The figure shows half-surface views (upper micrographs) and side views (lower micrographs) in (a) monolithic porcelain and in bilayers with porcelain coating thicknesses $d =$ (b) 670 μm, (c) 490 μm, and (d) 230 μm.

The load $P = 1000$ N chosen for illustration in Fig. 2 produces relatively heavy damage, enabling clear identification of the damage modes. Multiple ring cracking is observed on all top surfaces, confirming that the load is well above threshold for this type of cracking. Some of the surface rings have developed into full cone cracks in the section views. Note that the well-developed cones in the specimens with thicker coatings [Figs. 2(b) and 2(c)] appear to have comparable geometries (i.e., lengths

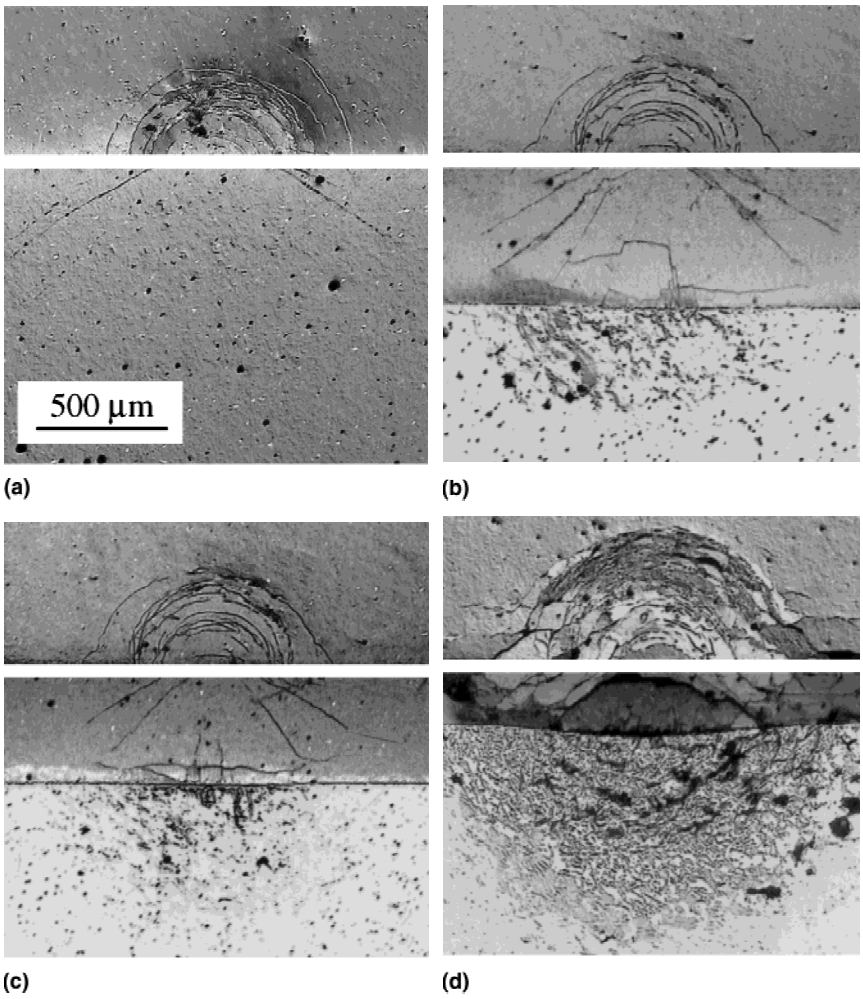

FIG. 2. Contact damage in porcelain/Pd-alloy coating/substrate bilayers, using WC sphere of radius $r = 2.38$ mm, at load $P = 1000$ N, coating thicknesses (a) $d = \infty$ (monolithic porcelain), (b) $d = 0.67$ mm, (c) $d = 0.49$ mm, (d) $d = 0.23$ mm. Bonded-interface specimens, showing top surface (upper) and section (lower) views.

and inclination angles) to those in the monolithic specimen [Fig. 2(a)], despite the appearance of yield in the metal substrates, suggesting that it is the cone crack that has formed first in these cases.

Yield zones in the substrate are well defined in the section views of all the bilayer specimens in Figs. 2(b)–2(d). The widths of the plastic zones are larger than those of the contact diameters on the coating surface, indicating substantial load transfer to the underlayer at the load $P = 1000$ N represented. Attendant upward extending median cracks are also apparent, especially in the thicker coatings [Figs. 2(b) and 2(c)]. Incipient laminar cracks parallel to the ceramic/metal interface but contained within the coating have begun to develop in Figs. 2(b) and 2(c), particularly in the latter. Observations of sections at lower loads, and in other coating thicknesses, indicate that substrate yield generally precedes median and laminar cracking in this particular ceramic/metal coating/substrate system.

In the specimen with the thinnest coating [Fig. 2(d)], the crack geometries are more complex, and the crack densities higher, indicating strong damage-mode interactions. The transverse cracks appear on the verge of penetrating through the coating sections. True interfacial delamination of the coating from the substrate is now evident. Note that the delamination is contained within the boundary of the yield zone. The coating is permanently depressed, foreshadowing complete failure of the coating.

B. Critical loads: Coating cone cracking

Figure 3 plots critical loads P_C for cone crack initiation in monolithic porcelain as a function of sphere radius r. Data for the two sphere radii used in the present study are shown as the filled symbols. Comparative data from an earlier study on another dental porcelain[30] are included as the unfilled symbols. The lines through the data sets are fits according to Auerbach's law, $P_C \propto r$.[32,33]

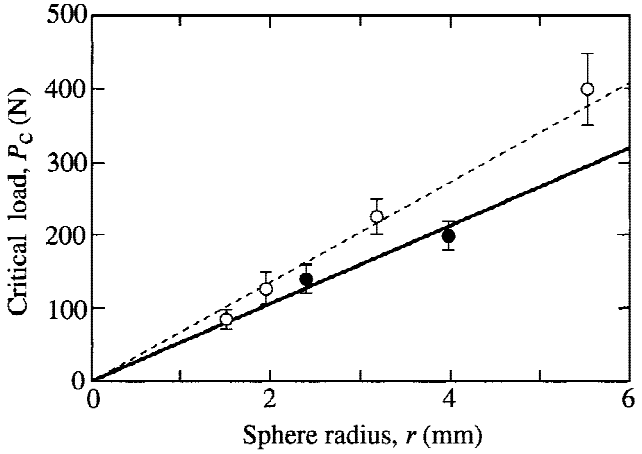

FIG. 3. Critical loads P_C for cone cracking in monolithic porcelain as function of WC sphere radius. Filled symbols are data from present study, unfilled symbols are data from previous study on another dental porcelain.[30] Error bars denote load range over which cone cracks first appear as short arcs and finally complete themselves as full circles about the contact. Solid line is linear fit, according to Auerbach's law.

The dependence of P_C on porcelain coating thickness d in the porcelain/Pd-alloy bilayers is shown in Fig. 4(a), for $r = 2.38$ and 3.98 mm. For each sphere radius, P_C diminishes monotonically with decreasing d, at first slowly and then more rapidly in the thin coating region as the load support progressively transfers from the coating to the substrate.

In accordance with the fits in Fig. 3, the data in Fig. 4(a) may be normalized for different sphere radii by plotting P_C/r versus d/r, Fig. 4(b). Included as the dashed curve in this plot are comparative results for a porcelain/alumina system (albeit a different porcelain) from an earlier study.[34] Note that the alumina substrate, although stiffer than the Pd-alloy (cf., $E = 250$ GPa for alumina, $E = 150$ GPa for alloy) appears to reduce P_C relative to the metal substrate system, especially at smaller d/r.

It is apparent that bilayers with thin coatings in contact with spheres are especially susceptible to this mode of damage.

C. Critical loads: Substrate yield

Figure 5 shows the depth h of the plastic zone in the substrate as a function of load P for porcelain/Pd-alloy bilayers with coating thicknesses, $d = 670$ μm, 490 μm, 330 μm, and 230 μm, as well as for monolithic metal ($d = 0$), for indenter radius $r = 2.38$ mm. The curves through the data sets are empirical fits. Extrapolation to $h = 0$ enables determination of the critical load P_Y for substrate yield at each value of d. These plots confirm that thicker brittle coatings afford greater protection against substrate deformation.

Figure 6 plots indentation stress–strain curves for bilayers of specified thicknesses d, as well as for constituent porcelain and Pd-alloy monoliths. The curve for monolithic porcelain exhibits a near-linear elastic behavior, with no evident quasi-plastic component, typical of highly brittle ceramics.[30] The curve for the Pd-alloy, on the other hand, shows a strong nonlinear curve with comparatively abrupt flattening, typical of highly ductile materials.[35] Note that the initial slope of the data for the Pd-alloy is distinctly higher than that for the porcelain, commensurate with relative Young's moduli ($E = 150$ GPa for metal, $E = 70$ GPa for porcelain). However, the metal is much softer above contact pressure ≈1 to 1.5 GPa, once yield occurs.

The indentation stress–strain curves for the bilayers lie intermediate between the monolithic bounds, tending more away from porcelain toward the metal with decreasing thickness.[23] Thus, the composite layer curves show slightly higher initial slope than the monolithic

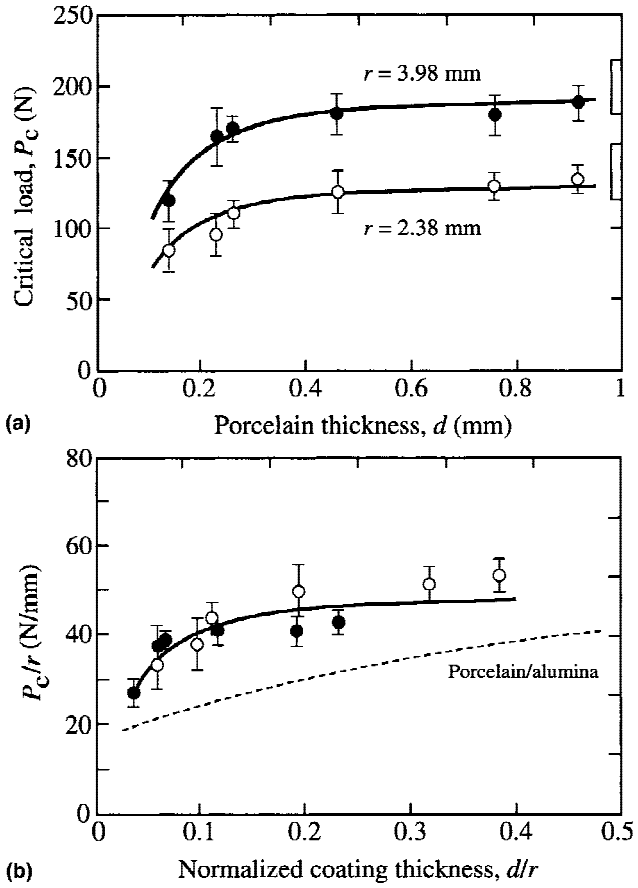

FIG. 4. (a) Plot of P_C versus d, for porcelain/Pd-alloy coating/substrate bilayers, showing data for sphere radii r indicated. Boxes at right indicate critical loads for monolithic porcelain. Error bars denote load range over which cone cracks first appear as short arcs and finally complete themselves as full circles about the contact. (b) Equivalent plot, with ordinates normalized to sphere radius r. Dashed curve is a fit to comparative data for porcelain/alumina bilayers, from Ref. 34.

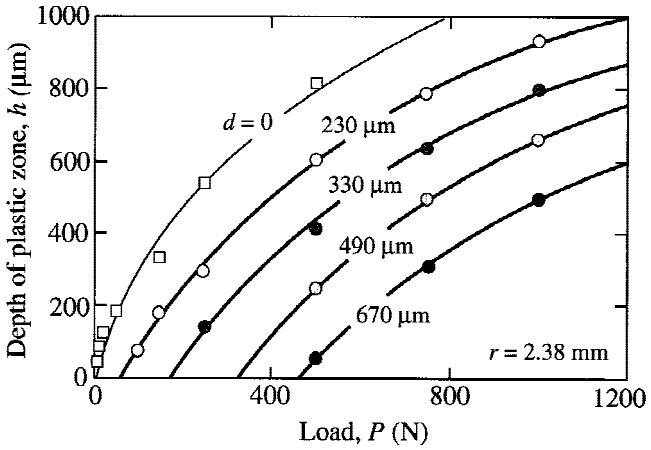

FIG. 5. Depth h of plastic zone in Pd-alloy substrate as function of load P, for WC sphere radius $r = 2.38$ mm and porcelain coating thicknesses $d = 670$ μm, 490 μm, 330 μm, 230 μm, and 0 (monolithic metal).

porcelain in the low-load elastic region, reflecting a stiffening effect from the substrate. However, the composite layer curves fall increasingly below the porcelain curve in the high-load substrate-yield region, more rapidly in the thinner coatings, as the load transfers to the substrate. The evolution of attendant median cracks in the thinner coatings enhances this decline in sustainable contact stress in the high load region.[23]

IV. DISCUSSION

We have demonstrated sphere-contact damage modes in a specific bilayer system, porcelain on Pd-alloy, in which the metal substrate is stiffer, but softer, than the ceramic coating. In the brittle coating, two basic transverse cracking modes are observed: (i) downward-extending cone cracks initiated from the top surface in the coating; (ii) upward-extending median cracks initiated from the lower surface (ceramic/metal interface) in the coating, preceded by yield in the substrate. The cone cracking mode has been well documented since the time of Hertz,[11,36] and typifies contact fractures on brittle monolithic or thick coating surfaces. The median cracking mode has only recently been described,[8,17,19,20,24,37–39] and constitutes the dominant mode in thinner brittle coatings on softer underlayers. A soft underlayer allows the coating to bend beneath the immediate contact, transforming the nature of the stress field away from ideal Hertzian toward that of plate flexure, allowing buildup of tensile stress at the lower coating surface. In the present metal system, the "softness" of the substrate is manifest only beyond the yield point,[20] indicating that a high Young's modulus is not sufficient guarantee for strong coating support; at least, not in thin coatings at high loads.

Following this last point, it is worth reiterating that laminar cracks in the coating, as with median cracks, are observed only after yield in the substrate. Such contact-induced laminar cracks are attributable to elastic spring-back in the ceramic coating relative to the irreversibly deformed substrate, a fact supported by observations that these cracks usually appear as the indenter is unloaded and remain laterally contained within the boundaries of the yield zone.[38] Initial laminar cracking occurs within the lower half of the coating thickness, immediately above the coating/substrate interface [Figs. 2(b) and 2(c)], and may be enhanced by the presence of weak internal boundaries associated with the sequential firing of the porcelain overlayers.[18] True delamination of the coating from the substrate occurs only after extensive substrate yielding [Fig. 2(d)].[18]

Critical loads P_C for initiation of coating cone cracking, Fig. 4, and P_Y for substrate yield, Fig. 5, have been measured as a function of coating thickness d for the porcelain/Pd-alloy bilayer system. At any given sphere radius r, both critical loads diminish as the coating thickness diminishes. We replot the critical load data for $r = 2.38$ mm on a composite design diagram in Fig. 7. Four regions may be distinguished: A, no cracking, no yielding ($P < P_C$, $P < P_Y$); B, cone cracking, no yielding ($P_C < P < P_Y$); C, yielding, no cone cracking ($P_Y < P < P_C$); D, cracking and yielding ($P > P_C$, $P > P_Y$). Region A is the domain of safe operation for damage-intolerant structures, in single-cycle contacts. In this domain, the key for the particular ceramic/metal system and sphere rep-

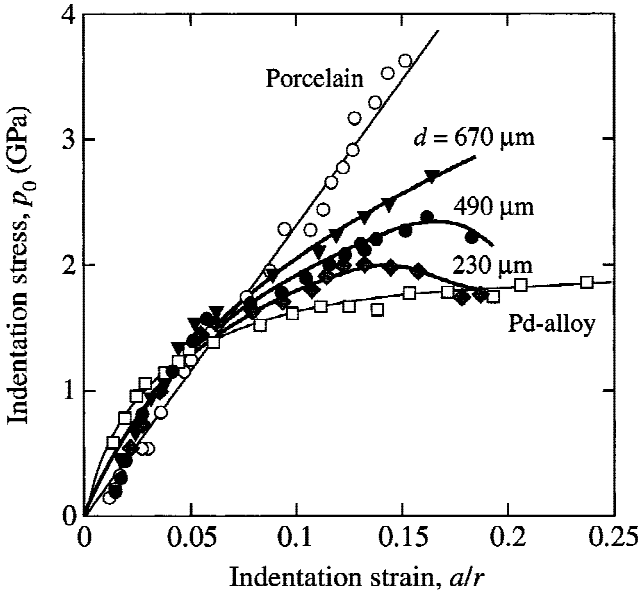

FIG. 6. Indentation stress–strain curves for porcelain/Pd-alloy coating/substrate bilayers with coating thicknesses (filled symbols) $d = 670$ μm, 490 μm, 230 μm, and (unfilled symbols) for monolithic porcelain and metal, for WC indenter radius $r = 2.38$ mm. (Data are subject to uncertainties of 5% from measurements of contact radius a.)

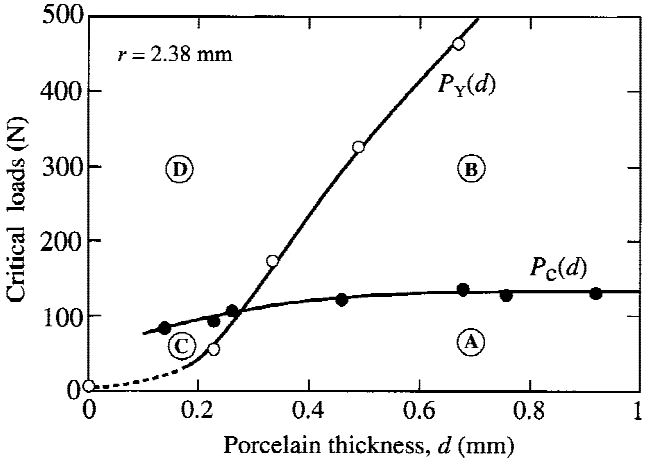

FIG. 7. Critical loads for cone cracking, P_C, and substrate yield P_Y, in porcelain/Pd-alloy bilayers, as a function of porcelain coating thickness *d*. Zones as follows: A, no cracking, no yielding (safe); B, cracking, no yielding; C, yielding, no cone cracking; D, cracking and yielding (imminent failure).

resented in Fig. 7 is to maintain the contact load below ≈100 N. Demands on the coating thickness *d* are less stringent, provided *d* remains above ≈300 μm. In damage-tolerant systems that can sustain some constrained coating cracking without operational failure (e.g., thermal barrier coatings),[3,4,38] it may be possible to operate in the higher-load region B, in which case thicker coatings would be advantageous. In thin film applications, it may be acceptable to extend into region C, provided the substrate yielding and associated median cracking in the coating is not sufficient to cause delamination. However, in applications where cyclic loading occurs (e.g., engine components, dental restorations), operation within region C is less tolerable, because of the susceptibility of metals to fatigue,[40] with the potential for accelerated cracking in the coating. The onset of nonlinearities in the stress–strain curves, e.g., Fig. 6, could provide a useful indicator for the onset of such yield. The region D of high loads and thin coatings, where both coating cracking and substrate yield occur [e.g., Fig. 2(d)], is clearly the most dangerous, with failure imminent.

The present study provides indications as to materials selection for metal layer structures with brittle coatings. Ideally, one would like the coating to be strong, to avoid cracking. In engine components, for example, high-strength fine-grain silicon nitrides[24] are the ceramics of choice. However, the strongest ceramic coatings may not always be practical because of restrictive operational factors, e.g., thermal insulation and corrosion protection in the case of thermal barrier coatings[3,4] and aesthetics in the case of dental restorations.[41] In damage-intolerant structures, one might also like the substrate to be stiff, to provide elastic support for the coating, and hard, to avoid yielding,[21] e.g., superalloys in engine components. A soft metal sublayer (or even polymeric sublayer, e.g., automobile windshields), on the other hand, may actually be preferable in instances where energy absorption is desirable. In other, damage-intolerant applications it may be advantageous to replace the substrate metal with a hard, high strength ceramic, to avoid substrate yielding altogether. In principle, this should extend region A in Fig. 7 to lower operational coating thicknesses. However, the use of a stiff ceramic sublayer may not always be beneficial: quite apart from the inherent brittleness of the ceramic sublayer itself, the critical loads for cone cracking in the outer coating may actually be diminished [e.g., as in the dashed curve for a porcelain/alumina bilayer system in Fig. 4(b)], because of local enhancement of concentrated tensile stresses in the near-contact surface region.[34]

A full description of the contact damage properties of ceramic/metal layer structures may involve factors beyond those covered in the present experiments. Mismatch in thermal expansion coefficients between the ceramic coating and metal substrate, by introducing residual compressive stresses in the coating,[26,27,42,43] can play a role by suppressing transverse fractures during contact.[24] (In dental restoration systems, including the porcelain/Pd-alloy used here, such potential benefits are forgone by choosing near-zero thermal expansion mismatch, to prevent spalling of porcelain layers from thermal shock during firing.) Repetitive loading may also intensify the damage, either by slow growth of the transverse coating cracks, or, more importantly, from mechanical fatigue of the yielding metal substrate. Aqueous environmental interactions may also be deleterious to cracking in the coating, although in order to be effective in enhancing median cracking any such environment would first need to gain access to the ceramic/metal interface.

As mentioned, porcelain/Pd-alloy layer systems are used routinely in the construction of porcelain-fused-to-metal dental crowns. The present results shed some light on the requirements for the reliable performance of such crowns. The domain of typical oral forces is <100 N,[6] although higher loads can be attained under severe biting conditions.[6,30] The cuspal radius at the biting contact typically lies between 2–4 mm.[30] Our present choices of load range and indenter radius encompass these values. From Fig. 7, we may anticipate that porcelain-fused-to-metal crowns should survive typical biting regimens provided the porcelain coating exceeds 300 μm or so. This is not inconsistent with a clinically recommended coating thickness of at least 0.5 mm, and ideally 1.0 mm.[6] Other dental crown systems with ceramic underlayers, e.g., porcelain-fused-to-alumina (porcelain jacket crown), offer greater stiffness (as well as superior aesthetics), but at the cost of increased brittleness. With crowns, the soft dentin interior of the underlying tooth structure

(modulus 10–20 GPa) may enhance the plate flexure mode of overlayer deformation; accordingly, a next step should be to investigate bilayer systems on soft polymeric substrates.

ACKNOWLEDGMENTS

The authors would like to thank D. Castaldini at Perth Dental Hospital and P. Chantler at the School of Oral Health Science, The University of Western Australia, for assistance in preparing the porcelain/Pd-alloy specimens. This work was supported by grants from the Australian Research Council and the United States National Institute of Dental Research.

REFERENCES

1. V.J. Laraia and A.H. Heuer, J. Am. Ceram. Soc. **72,** 2177 (1989).
2. J.C. Knight, T.F. Page, and I.M. Hutchings, Thin Solid Films **177,** 117 (1989).
3. R.A. Miller, Surf. Coat. Technol. **30,** 1 (1987).
4. H. Herman, C.C. Berndt, and H. Wang, in *Ceramic Films and Coatings*, edited by J.B. Wachtman and R.A. Haber (Noyes Publications, Park Ridge, NJ, 1993), p. 131.
5. Y. Akimune, Y. Katano, and K. Matoba, J. Am. Ceram. Soc. **72,** 1422 (1989).
6. J.R. Kelly, Ann. Rev. Mater. Sci. **27,** 443 (1997).
7. Y.G. Jung, S. Wuttiphan, I.M. Peterson, and B.R. Lawn, J. Dent. Res. **78,** 887 (1999).
8. H.M. Chan, Ann. Rev. Mater. Sci. **27,** 249 (1997).
9. K.L. Johnson, *Contact Mechanics* (Cambridge University Press, London, 1985).
10. B.R. Lawn, N.P. Padture, H. Cai, and F. Guiberteau, Science **263,** 1114 (1994).
11. B.R. Lawn, J. Am. Ceram. Soc. **81,** 1977 (1998).
12. K. Komvopolous, ASME J. Tribology **111,** 430 (1989).
13. H. Gao, C-H. Chiu, and J. Lee, Int. J. Solids Struct. **29,** 2471 (1992).
14. M.V. Swain and J. Mencik, Thin Solid Films **253,** 204 (1994).
15. D.F. Diao, K. Kato, and K. Hokkirigawa, Trans. ASME J. Tribology **116,** 860 (1994).
16. Y. Sun, A. Bloyce, and T. Bell, Thin Solid Films **271,** 122 (1995).
17. L. An, H.M. Chan, N.P. Padture, and B.R. Lawn, J. Mater. Res. **11,** 204 (1996).
18. A. Pajares, L. Wei, B.R. Lawn, N.P. Padture, and C.C. Berndt, Mater. Sci. Eng. A **208,** 158 (1996).
19. A.C. Fischer-Cripps, B.R. Lawn, A. Pajares, and L. Wei, J. Am. Ceram. Soc. **79,** 2619 (1996).
20. S. Wuttiphan, B.R. Lawn, and N.P. Padture, J. Am. Ceram. Soc. **79,** 634 (1996).
21. S. Wuttiphan, A. Pajares, B.R. Lawn, and C.C. Berndt, Thin Solid Films **293,** 251 (1997).
22. T.J. Lardner, J.E. Ritter, and G-Q. Zhu, J. Am. Ceram. Soc. **80,** 1851 (1997).
23. X.Z. Hu and B.R. Lawn, Thin Solid Films **322,** 225 (1998).
24. K.S. Lee, S.K. Lee, B.R. Lawn, and D.K. Kim, J. Am. Ceram. Soc. **81,** 2394 (1998).
25. H. Chai and B.R. Lawn, J. Mater. Res. **14,** 3805 (1999).
26. O. Prakash, P. Sarkar, and P.S. Nicholson, J. Am. Ceram. Soc. **78,** 1125 (1995).
27. H. Wang and X.Z. Hu, J. Am. Ceram. Soc. **79,** 553 (1996).
28. F. Guiberteau, N.P. Padture, and B.R. Lawn, J. Am. Ceram. Soc. **77,** 1825 (1994).
29. H. Cai, M.A. Stevens Kalceff, and B.R. Lawn, J. Mater. Res. **9,** 762 (1994).
30. I.M. Peterson, A. Pajares, B.R. Lawn, V.P. Thompson, and E.D. Rekow, J. Dent. Res. **77,** 589 (1998).
31. F. Guiberteau, N.P. Padture, H. Cai, and B.R. Lawn, Philos. Mag. A **68,** 1003 (1993).
32. F.C. Frank and B.R. Lawn, Proc. Roy Soc. Lond. A **299,** 291 (1967).
33. B.R. Lawn, *Fracture of Brittle Solids* (Cambridge University Press, Cambridge, United Kingdom, 1993), Chap. 8.
34. S. Wuttiphan, PhD Thesis, University of Maryland (1997).
35. A.C. Fischer-Cripps and B.R. Lawn, J. Am. Ceram. Soc. **79,** 2609 (1996).
36. H. Hertz, *Hertz's Miscellaneous Papers* (Macmillan, London, 1896).
37. H. Liu, B.R. Lawn, and S.M. Hsu, J. Am. Ceram. Soc. **79,** 1009 (1996).
38. A. Pajares, L. Wei, B.R. Lawn, and C.C. Berndt, J. Am. Ceram. Soc. **79,** 1907 (1996).
39. K.S. Lee, S. Wuttiphan, X.Z. Hu, S.K. Lee, and B.R. Lawn, J. Am. Ceram. Soc. **81,** 571 (1998).
40. S. Suresh, *Fatigue of Materials* (Cambridge University Press, Cambridge, 1991).
41. K.J. Anusavice, *Phillips' Science of Dental Materials* (Saunders, Philadelphia, PA, 1996).
42. A.V. Virkar, J.L. Huang, and R.A. Cutler, J. Am. Ceram. Soc. **70,** 164 (1987).
43. R. Sathyamoorthy, A.V. Virkar, and R.A. Cutler, J. Am. Ceram. Soc. **75,** 1136 (1992).